J Solid State Electrochem (2010) 14:1719–1726
DOI 10.1007/s10008-010-1022-z

ORIGINAL PAPER

Synthesis, characterization, and electrochemical properties of self-assembled leaf-like CuO nanostructures

Mushtaq A. Dar · Sang H. Nam · Youn S. Kim · Won Bae Kim

Received: 15 October 2009 / Revised: 27 January 2010 / Accepted: 29 January 2010 / Published online: 25 February 2010

Abstract A simple hydrothermal process was used to synthesize the assembled leaf-like copper oxide (CuO) from copper hydroxide and urea in aqueous solution. The field emission scanning electron microscopy revealed that the individual CuO leaf-like nanostructure has a dimension of about 0.5–1.5 μm in length, 50–70 nm in thickness, and 80–110 nm in width, respectively. These CuO nanostructures were structurally characterized by X-ray diffraction and Raman spectroscopy, which showed that the CuO nanostructures prepared from the hydrothermal process have high crystalline properties with a monoclinic structure. X-ray photoelectron spectroscopy studies confirmed that the as-prepared sample is composed of CuO, which is consistent with X-ray diffraction patterns. The CuO nanostructures were used as electrode materials for lithium-ion batteries, demonstrating electrochemical properties of a high initial discharge capacity of approximately 1,028 mAh/g along with good cycle stability.

Keywords X-ray diffraction · Nanostructures · CuO · Hydrothermal process · Transmission electron microscopy

Introduction

Large-scale self-assemblies of meso-, micro-, and nano-structured building blocks have attracted a significant interest due to its promising applications in recent years [1–4]. Substantial efforts have been made to fabricate hierarchical and complex structures that are assembled by nanoparticles, nanorods, and nanobelts as the building blocks [5, 6]. Self-organization of such components is a key step for the fabrication of nano- and microstructures and for the realization of device applications [7, 8]. Semiconducting metal oxide nanostructures having a tailored architecture are of importance in the field of nanotechnology research area [9]. Among them, cupric oxide (CuO) is a useful material with diverse applications to semiconductors [7], gas sensors [8, 14], battery electrodes [10, 11] and materials for memory devices [12], and field effect transistors [13]. CuO has a monoclinic structure in which each Cu atom has four nearest neighbors of oxygen atoms and exists at the center of oxygen rectangular, while oxygen atoms are located at the center of distorted tetrahedron of Cu [15]. CuO is also a p-type semiconductor with a narrow band gap of about 1.2 eV [16]. Nanoscale materials are of great interest with potential applications in nanodevices due to its unique optical, electrical, and magnetic properties [17, 18]. CuO nanostructures are therefore expected to have novel properties superior to their bulk phase counterparts. In particular, a variety of CuO nanostuructures have been prepared by high-temperature approaches. However, low-temperature hydrothermal process should be more versatile for the preparation of nanostructured CuO in temperatures ranging from 100 to 200 °C [19, 20].

Herein, we report a hydrothermal synthetic method and physicochemical characterization of self-assembled CuO nanostructures with leaf-like shape. Moreover, these leaf-like CuO nanostructures show an excellent electrochemical behavior as an electrode of rechargeable lithium-ion batteries with a high capacity and good cycle stability.

M. A. Dar · S. H. Nam · Y. S. Kim · W. B. Kim (✉)
Department of Materials Science and Engineering,
Gwangju Institute of Science and Technology (GIST),
261 Cheomdan-gwagiro, Buk-gu,
Gwangju 500-712, South Korea
e-mail: wbkim@gist.ac.kr

Experimental

Preparation of assembled leaf-like CuO nanostructures

All the chemical reagents used in this experiment were analytical grade. A typical procedure for the synthesis of CuO nanostructures is described as follows: A copper precursor solution (0.1 M) was prepared by mixing copper (II) hydroxide ($Cu(OH)_2$, 90%, Junsei Chemical Co., Ltd.) in a double distilled water. A solution (0.1 M) of urea ($CO(NH_2)_2$, 99.5%, Sigma Aldrich Co., Ltd.) was added to the copper solution under continuous stirring. Then, the mixture was transferred into a Teflon-lined stainless steel autoclave. The autoclave was sealed and maintained at a temperature of 150 °C for 6–12 h. After the reactions, the autoclave reactor was cooled down to room temperature. The obtained black-colored precipitate was washed several times with ethanol and double distilled water to ensure that the dissolved inorganic ions are removed and then dried at 75 °C for 12 h.

The formation of leaf-like CuO in the reaction system can be presented by the following reactions:

$$CO(NH_2)_{2(s)} + 3H_2O(aq) \rightarrow 2NH^+_{4\,(aq)} + 2OH^-_{(aq)} + CO_{2(g)}$$

$$Cu(OH)_{2(s)} \rightarrow CuO_{(s)} + H_2O_{(aq)}.$$

In this reaction, the urea acts as pH buffer and provides steady OH^- ions through the hydrolysis of water.

Physicochemical characterizations

X-ray diffraction (XRD) analysis was carried out by a powder diffractometer (Rigaku III/A, Japan) equipped with a copper target and a nickel filter to analyze the structure of the grown product. Field emission scanning electron microscopy (FESEM) (Hitachi, Japan), which was outfitted with X-ray energy dispersion spectrum, was employed to examine the morphology and elemental analysis of the as-grown products. Detailed microstructural analysis was performed by transmission electron microscopy (TEM; Hitachi model JEM-2010) together with selected electron diffraction at an accelerating voltage of 200 kV. Fourier transform infrared (FTIR) was recorded in the wave-numbers of 300–2,000 cm^{-1}. For chemical composition analysis, X-ray photoelectron spectroscopy (XPS) studies were carried out with an AXIS-NOVA (Kratos) system using $Al_{K\alpha}$ (150 W) radiation. Raman spectra were collected on a FT-Raman spectrometer (RFS 100/S, Bruker) using Nd:YAG laser at 1,064 nm. The power at the CuO sample was estimated to be 80 mW. The overall resolution of about 4 cm^{-1} was possible with this spectrometer. The thermogravimetric measurements of the as-grown CuO nanostructures were carried out on a TGA-2050 thermogravimetric analyzer from 20 to 700 °C at a nitrogen flow rate of 60 ml/min at a heating rate of 10 °C/min.

Electrochemical properties of the leaf-like CuO nanostructures

The electrochemical properties of the as-grown leaf-like CuO nanostructures were investigated using two-electrode coin-type cells (CR2032). For electrode fabrication, 20 mg of the obtained CuO nanostructures was mixed with 12 mg of a mixture of conductive binder that consists of 8 mg of Teflonized acetylene black and 4 mg of graphite [21]. The mixture was pressed on a nickel foam which was used as the current collector and dried at 100 °C for 10 h in a vacuum oven. The cell was composed of the CuO electrode and metallic lithium as the working and counter electrode, respectively, in which they were separated by a porous polypropylene separator. The electrolyte was a 1 M $LiPF_6$-ethylene carbonate (EC)-dimethyl carbonate (in 1:1 volume). The cells were assembled in an argon-filled dry box and tested at room temperature. The electrochemical performances of the CuO nanostructure electrodes were examined by galvanostatic discharge/charge measurement. These cells were cycled using a WBCS 3000 battery cycler system (Won-A Tech corp.). The electrochemical potential cycling tests were performed using an AUTOLAB (ECO CHEMIE) cell test system. Continuous potential cycling over the leaf-like CuO nanostructure electrodes was carried out for up to 30 cycles in the potential range of 0.01–3 V at a scan rate of 0.02 mV/s.

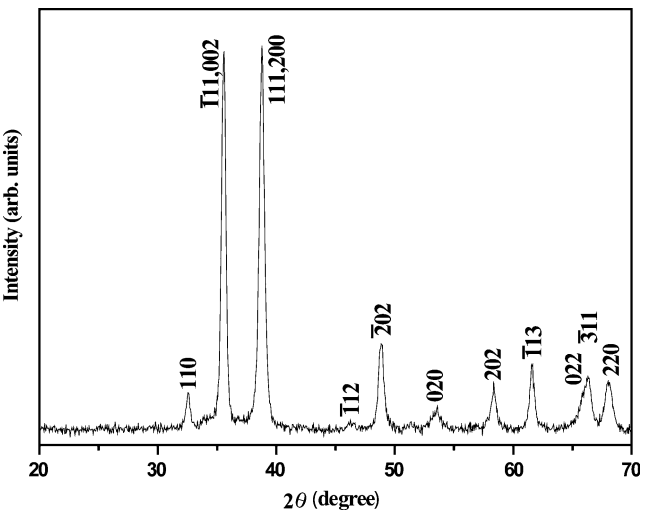

Fig. 1 XRD analysis of CuO nanostructures

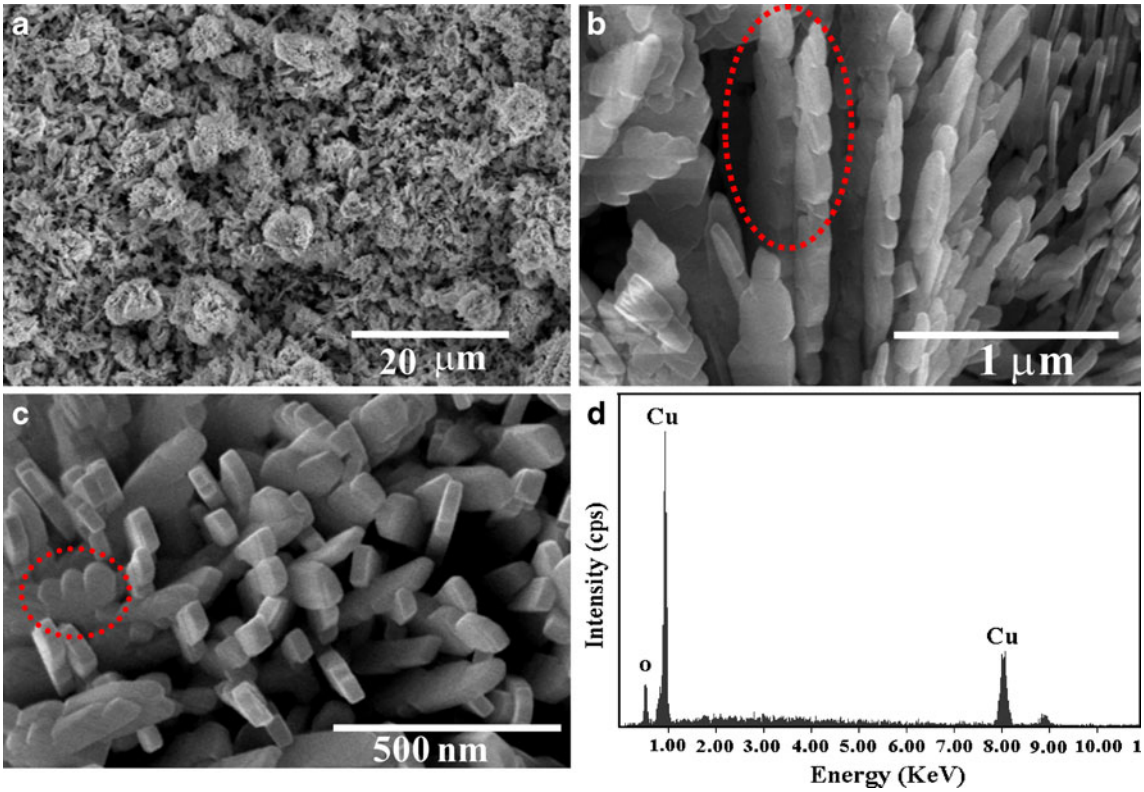

Fig. 2 Low magnification (**a**), tilted view (**b**), top view FESEM images (**c**), and EDX spectra of the leaf-like CuO nanostructures (**d**)

Result and discussion

Characterization of materials

A typical XRD pattern of the as-synthesized CuO nanostructures is shown in Fig. 1. All the diffraction peaks can be indexed to the monoclinic structure of CuO (space group $C2/c$; a_0=4.683 Å, b_0=3.422 Å, c_0=5.128 Å, and β= 99.54°; JCPDS card no. 72-0629) [22, 23]. No other impurity phases except the crystalline CuO phase were detected by XRD analysis, indicating a good phase purity of the leaf-like CuO nanostructures prepared here. The strong diffraction peak intensities also suggest that the leaf-like CuO nanostructures are in a highly crystalline nature.

In order to examine the microstructure and surface morphology of CuO nanostructures, FESEM was performed. Figure 2a shows a representative morphology at a low magnification of the leaf-like CuO nanostructures, revealing a large population of the CuO assemblies with nano-leaves. High-magnification images of the leaf-like CuO exhibit one-dimensional structures of the CuO nano-leaves, as seen in Fig. 2b, c; they are constituted to form the CuO assemblies in Fig. 2a. Each array of the leaf-like CuO is about 500 nm–1.5 μm in length, 50–70 nm in thickness, and 80–110 nm in width, respectively. The tips of these leaf-like CuO appear to be sharp and possess uniform lengths and widths. The X-ray energy-dispersive analysis (EDX) indicates the signals from Cu and O elements (Fig. 2d),

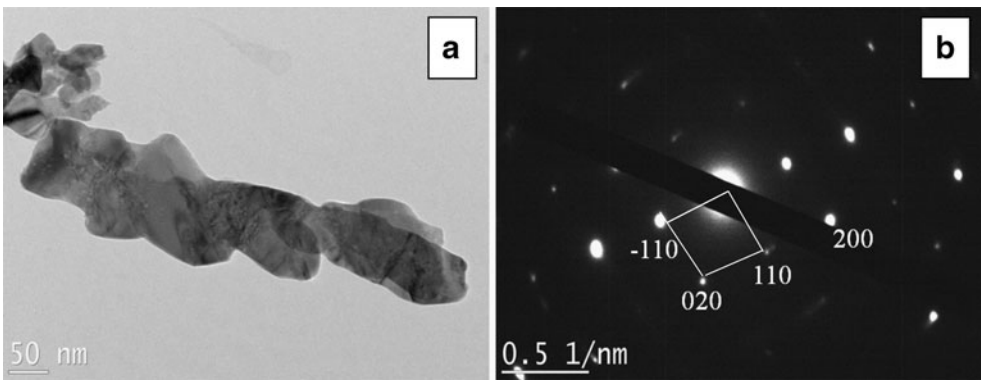

Fig. 3 TEM analysis of the grown leaf-like CuO nanostructures: low-magnification TEM image (**a**) and selected area electron diffraction pattern (**b**)

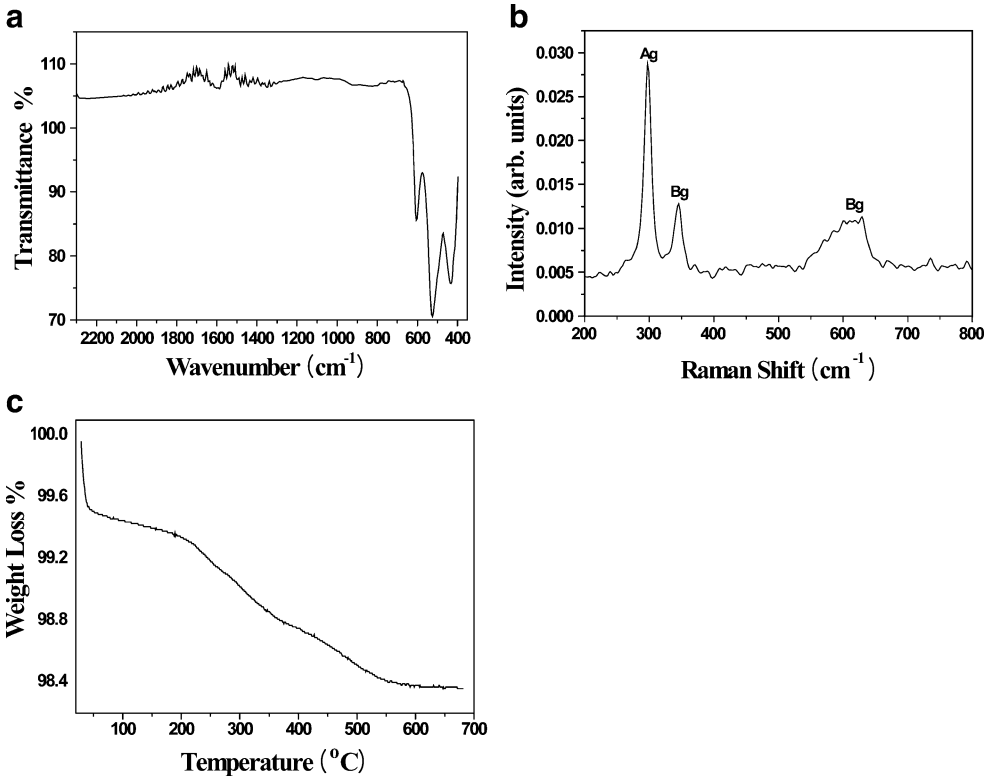

Fig. 4 FTIR spectra (**a**), Raman spectra (**b**), and TGA curve of the leaf-like CuO nanostructures under a nitrogen flow at a heating rate of 10 °C/min (**c**)

revealing that the Cu and O are present in a stoichiometric ratio, thus verifying the purity of the CuO phase. Furthermore, microstructural analysis of CuO nanostructures was performed using TEM, which represents the self-organized architecture of CuO nanostructures as shown in Fig 3a. Selective area electron diffraction pattern in Fig. 3b also indicates the single crystalline phase of the leaf-like CuO nanostructure, which accords well with the XRD results. The TEM micrographs are in good agreement with the previous FESEM and XRD results.

Figure 4a shows FTIR spectra of the obtained CuO nanostructures. The characteristic peaks positioned at around 606 and 525 cm^{-1} were observed due to Cu–O stretching along the [−202] direction and 432 cm^{-1} from Cu–O stretching along the [202] direction [24].

Raman spectroscopy is known to be a very useful tool for monitoring the structural order–disorder degree at short range and crystallinity of oxide materials.

Raman spectra of the leaf-like CuO nanostructures are illustrated in Fig. 4b. The peak broadens and shifts to the lower frequency side as the size of the microcrystal decreases [25]. The monoclinic CuO belongs to the C_{2h}^6 space group with two molecules per unit cell. There are nine zone centers in optical phonon modes with symmetries of $4A_u + 5B_u + A_g + 2B_g$. The ($A_g + 2B_g$) modes are Raman active [26, 27]. A broad peak with a relatively high intensity at 297.5 cm^{-1} is assigned to A_g band, and two peaks at 345.6 and 629 cm^{-1} are assigned to $2B_g$. The observed peaks of Raman active modes on this sample are in good agreement with the previous reports (Table 1). These significant peak intensities indicate the single phase property and high crystallinity of as-grown leaf-like CuO structures.

Figure 4c shows the TGA analysis of CuO nanostructures in which a total weight loss of about 1.73% can be seen as the temperature is increased up to 700 °C. The initial weight loss is observed at temperatures below 50 °C, and a further weight loss appears from approximately 245 °C. The latter weight loss is probably attributed to the formation of CuO from its unreacted precursors [32, 33]. The weight loss

Table 1 Raman modes of the CuO nanostructures

Preparation method	(Ag + 2Bg) (cm^{-1})	Temperature (K)	Time (h)	Reference
Hydrothermal	297/346/631	373–423	6–12	[28]
Microwave hydrothermal	283.8/333.5/622.5	393	1	[29]
Thermal CVD	291/340/623	573–973	2	[30]
Hydrothermal	296/342/627	393	·30	[31]
Hydrothermal	297.5/345.6/629	423	6–12	This work

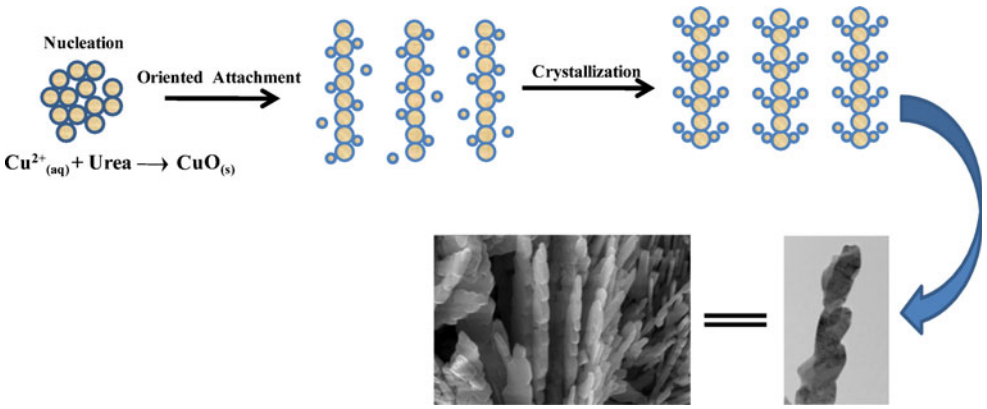

Fig. 5 Schematic diagram for the formation of leaf-like CuO nanostructures

observed in this sample is small, implying thermal stability of the CuO sample.

Figure 5 shows the schematic diagram of growth mechanism for the formation of leaf-like CuO nanostructures. In principle, there are three basic steps for the formation of CuO nuclei during the precipitation process. The first is to initiate by producing building units in solution for a nucleation phase. The concentration of building units in solution increases until a significant supersaturation level is reached, and then the nucleation process takes place [34]. The CuO nuclei formed serve as the building blocks for the formation of CuO nanostructures [35]. In the process of oriented aggregation, the single crystalline CuO nano-leaves are formed through an oriented attachment by rotating adjacent nanoparticles to share an identical crystallographic orientation [36]. The formation of the leaf-like CuO nanostructures in this work may occur via a rapid nucleation by dehydration of $Cu(OH)_2$ and followed by the oriented aggregation-based growth of CuO nuclei for their crystal growth. The reactant concentrations, pH, temperature, and reaction time could affect the growth and formation processes of the leaf-like CuO structures.

To scrutinize the composition and purity of the as-prepared product, the XPS study was carried out. Figure 6a depicts a high sensitivity (survey spectrum) scan with the presence of Cu and O elements. No other obvious impurities were found in the spectrum except low-intensity peak of carbon, which might result from the

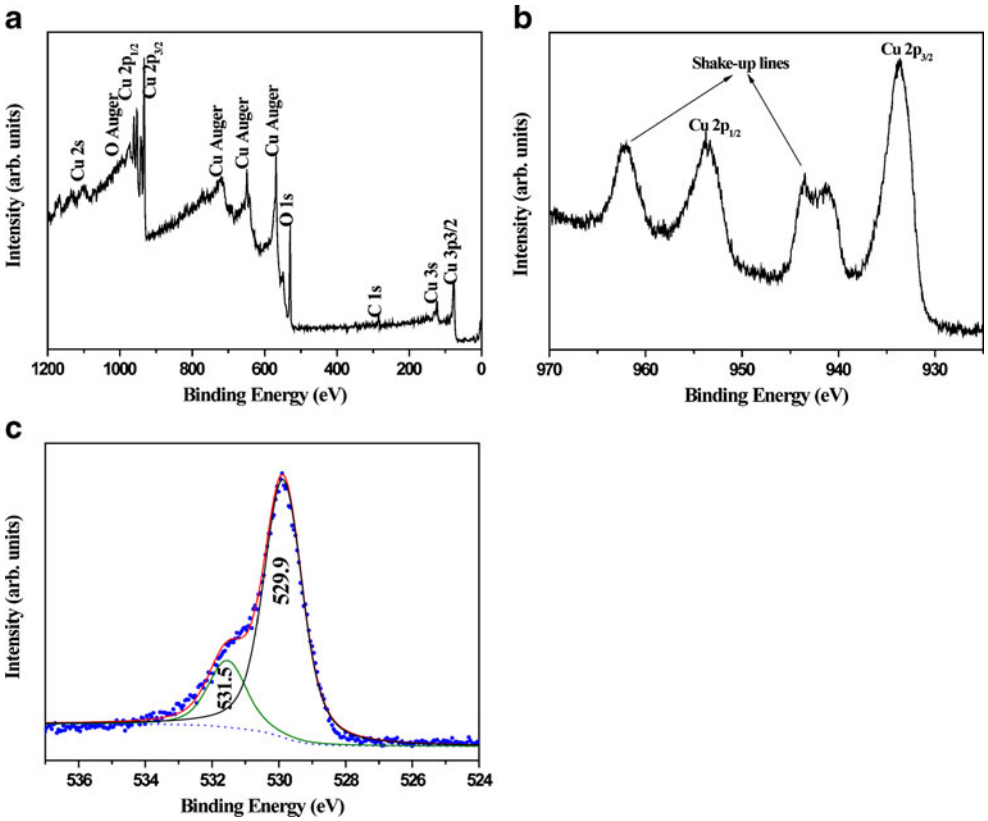

Fig. 6 XPS survey scan spectrum of the leaf-like CuO nanostructures (**a**). Close-up surveys for Cu 2p core (**b**). Core-level O 1s spectrum of CuO (**c**); the dotted curve is the experimental data and solid lines are the result of curve-fitting procedure

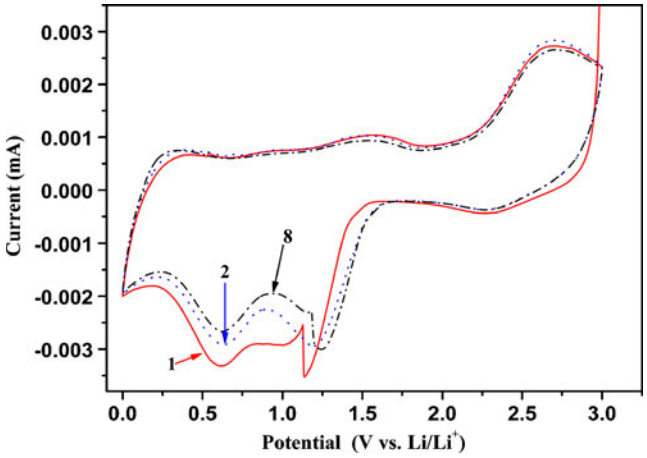

Fig. 7 Cyclic voltammograms of the CuO nanostructure electrode at a scan rate of 0.02 mV/s

surface contamination [37]. The Cu 2p peak of the leaf-like CuO nanostructures is illustrated in detail in Fig. 6b. The Cu $2p_{3/2}$ lies at 933.65 eV with a shake-up satellite at about 943.2 eV and Cu $2p_{1/2}$ lies at 953.5 eV with a satellite at about 962 eV, which is consistent with earlier reports [38]. The presence of shake-up satellite features for Cu 2p rules out the possibility of the presence of Cu_2O phase [39]. The gap between Cu $2p_{1/2}$ and Cu $2p_{3/2}$ is about 20 eV, which is in agreement with the standard spectrum of CuO. In Fig. 6c, the O 1s core-level spectrum is broad, and two O 1s peaks can be resolved using curve-fitting procedure. The binding energies have been identified as O^{2-} in CuO at 529.9 eV [40], and oxygen adsorbed on the surface of CuO at 531.5 eV. Thus, the XPS result clearly proved that the acquired black powder is only composed of CuO, which is consistent with the XRD results.

Electrochemical properties of the leaf-like CuO nanostructures

Cyclic voltammetry (CV) measurements were used to investigate the reversibility of the CuO nanostructure electrodes during the discharge–charge processes with lithium ions at a scan rate of 0.02 mV/s. Figure 7 shows the first, second, and eighth cyclic voltammograms for the as-grown CuO nanostructure electrode. Two reduction peaks at the potentials of approximately 1.13 and 0.62 V can be observed in the first scan, while only one dominant oxidation peak with shoulder appears to evolve at about 2.68 V [41]. In the subsequent cycles, the intensities of the peaks slightly decrease, and the cathodic peaks at 1.13 V seems to be shifted to 1.18 V at the second cycle and further shifted to 1.25 V for the eighth cycles. However, the intensity and position of the peaks can be assumed to remain almost constant, probably implying a good cycle stability of the CuO nanostructured electrode [42].

The 1st, 2nd, 3rd, 10th, and 30th discharge–charge curves of the CuO nanostructure electrode are depicted in Fig. 8a. In the first discharge process of CuO nanostructure, three discharge plateaus are observed at the potential ranges of 2.7–1.8, 1.4–1.1, and 0.8–0.6 V. During the second discharge process, all the slopes become larger and the plateau at 2.70–1.80 V shifts slightly upward. As seen in Fig. 8b, the CuO electrodes exhibit initial insertion capacities of about 1,028 mAh/g and extraction capacity of about 580 mAh/g. As expected for nanomaterials in lithium-ion batteries, the CuO nanostructure electrode also shows a large irreversible capacity loss in the first cycle, which can be attributed to the electrolyte decomposition [10, 11], the reduction of surface groups, and the formation of lithium oxide [43]. Multi-discharge plateaus indicate that multistep electrochemical reactions may be involved during the discharge–charge process. There may be a series of insertion and decomposition reactions of CuO with Li^+ during the discharge and charging process. The first process corresponds to the continuous reduction of the Cu(II) species to Cu(I) and finally to Cu(0), and the second process corresponds to the catalytic decomposition of liquid electrolyte to form a solid electrolyte interphase at such a low voltage [44]. The initial discharge capacity of the CuO nanostructure was estimated to approximately 1,028 mAh/g.

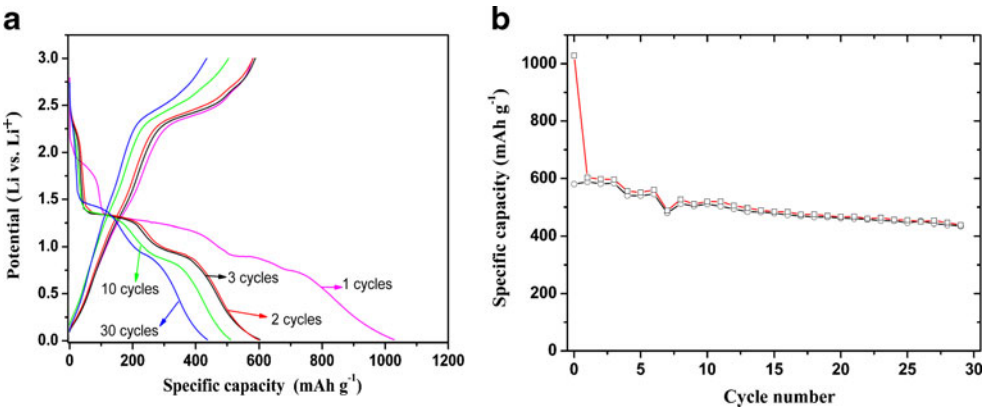

Fig. 8 Discharge-charge curves (**a**). Specific capacity of the CuO nanostructure electrode as a function of cycling number (**b**)

The irreversible capacity in the first process could be originated from the decomposition of electrolyte and consequential formation of an organic layer deposited on the surface of particle, which occurs in the low-potential region for transition metal oxides [45]. The irreversible capacity generated from the formation of lithium oxide noticeably decreases in the second cycle [43]. The discharge capacity of CuO nanostructure would be relatively smaller as compared to the results reported by Gao et al. [46, 47] in which polycrystalline CuO nanocrystals were used with a larger surface area and a smaller size (quantum size effect). However, our results are comparable to the results obtained using CuO nanoplatelets [48]. In summary, these self-assembled leaf-like CuO nanostructures demonstrated good electrochemical performances with a specific capacity of about 440 mAh/g even after 30 cycles with a slow capacity fading rate.

Conclusions

In summary, a hydrothermal process was used to synthesize the CuO assembly with leaf-like nanostructures from copper hydroxide and urea in aqueous solution. From the several physicochemical characterizations, it was shown that the leaf-like CuO nanostructures are 500 nm to 1.5 μm in length, 50–70 nm in thickness, and 80–110 nm in width, respectively. Further structural analysis showed that the CuO nanostructures have a high crystalline nature in the monoclinic crystal structure. Raman spectra revealed three bands at 296, 345, and 629 cm^{-1} that correspond to the Ag, Bg1, and Bg2 modes of the cupric oxide. TGA analysis illustrated a good thermal stability. X-ray photoelectron spectroscopy studies clearly proved that the as-prepared sample is composed of CuO. A possible growth mechanism is proposed for the formation of leaf-like CuO nanostructures. The leaf-like CuO nanostructures demonstrated a good electrochemical performance with a specific capacity of about 440 mAh/g after 30 cycles with a slow fading rate and may attain prominent applications in high-performance lithium ion batteries.

Acknowledgments This work was supported by the Korea Science and Engineering Foundation (KOSEF) NCRC grant funded by the Korea government (MEST, no. R01-2008-006-03002-0) and National Research Foundation of Korea (NRF) grant funded by the Korea government (MEST, no. 20090058918). M. A. Dar greatly acknowledges the support from the BK-21 Program.

References

1. Kohiki S, Takada S, Yamada K, Adachi Y, Shimizu A, Oku M, Mitome M (2000) Physica E 5:161–166
2. Cavalcante LS, Sczancoski JC, Lima LF Jr, Espinosa JWM, Pizani PS, Varela JA, Longo E (2009) Cryst Growth Des 9:1002–1012
3. Qu X-R, Jia D-C (2009) J Cryst Growth 311:1223–1228
4. Sczancoski JC, Bomio MDR, Cavalcante LS, Joya MR, Pizani PS, Varela JA, Longo E, Li MS, Andrés JA (2009) J Phys Chem C 113:5812–5822
5. Liu J, Huang X, Li Y, Li Z, Chi Q, Li G (2008) Solid State Sci 10:1568–1576
6. Chen L, Li L, Li G (2008) J Alloys Compd 464:532–536
7. MacDonald AH (2001) Nature 414:409–410
8. Zhang JT, Liu JF, Peng Q, Wang X, Li YD (2006) Chem Mater 18:867–871
9. Eliziário SA, Cavalcante LS, Sczancoski JC, Pizani PS, Varela JA, Espinosa JWM, Longo E (2009) Nanoscale Res Lett 4:1371–1379
10. Chen LB, Lu N, Xu CM, Yu HC, Wang TH (2009) Electrochim Acta 54:4198–4201
11. Wang H, Pan Q, Zhao J, Chen W (2009) J Alloys Compd 476:408–413
12. Zhou P, Lv HB, Yin M, Tang L, Song YL, Tang TA, Lin Y (2008) J Vac Sci Technol B 26:1030–1032
13. Liao L, Zhang Z, Yan B, Zheng Z, Bao QL, Wu T, Li CM, Shen ZX, Zhang JX, Gong H, Li JC, Yu T (2009) Nanotechnology 20:085203
14. Yamamoto K, Kasuga T, Nogami M (1999) Electrochem Solid-State Lett 2:595–596
15. Xu JZ, Zhu JJ, Wang H, Chen HY (2003) Anal Lett 36:2723–2733
16. Kaur M, Muthe KP, Despande SK, Choudhury S, Singh JB, Verma N, Gupta SK, Yakhmi JV (2006) J Cryst Growth 289:670–675
17. Favier F, Walter EC, Zach MP, Benter T, Penner RM (2001) Science 293:2227–2231
18. Ghijsen J, Tjeng LH, Van Elp J, Eskes H, Westerink J, Sawatzky GA (1988) Phys Rev B 38:11322–11330
19. Liu Q, Liu H, Liang Y, Xu Z, Yin G (2006) Mater Res Bull 41:697–702
20. Yang Q, Yan PX, Chang JB, Feng JJ, Yue GH (2006) Phys Lett A 361:493–496
21. Song CH, Stephan AM, Lee YS, Nahm KS (2007) Mater Chem Phys 101:63–68
22. Yu H, Yu J, Liu S, Mann S (2007) Chem Mater 19:4327–4334
23. Keyson D, Volanti DP, Cavalcante LS, Simoes AZ, Varela JA, Longo E (2008) Mater Res Bull 43:771–775
24. Xu YY, Chen DR, Jiao XL (2005) J Phys Chem B 109:13561–13566
25. Tanaka A, Onari S, Arai T (1992) Phys Rev B 45:6587–6592
26. Wang Z, Pischedda V, Saxena SK, Lazor P (2002) Solid State Commun 121:275–279
27. Xu JF, Ji W, Shen ZX, Tang SH, Ye XR, Jia DZ, Xin XQ (1999) J Solid State Chem 147:516–519
28. Dar MA, Ahsanulhaq Q, Kim YS, Sohn JM, Kim WB, Shin HS (2009) Appl Surf Sci 255:6279–6284
29. Volanti DP, Keyson D, Cavalcante LS, Simoes AZ, Joya MR, Longo E, Varela JA, Pizani PS, Souza AG (2008) J Alloys Compd 459:537–542
30. Chou MH, Liu SB, Huang CY, Wu SY, Cheng CL (2008) Appl Surf Sci 254:7539–7543
31. Wang X, Xi G, Xiong S, Liu Y, Xi B, Yu W, Qian Y (2007) Cryst Growth Des 7:930–934
32. Sharma AK (2006) J Environ Eng 132:956–959
33. Zhang M, Xu X, Zhang M (2008) Mater Lett 62:385–388
34. Ahsanulhaq Q, Kim SH, Kim JH, Hahn YB (2008) Mater Res Bull 43:3483–3489
35. Ahsanulhaq Q, Umar A, Hahn YB (2007) Nanotechnology 18:115603
36. Yang R, Gao L (2005) Solid State Commun 134:729–733
37. Zeng DW, Yung KC, Xie CS (2003) Appl Surf Sci 217:170–180

38. Wang QH, Corrigan TD, Dai JY, Chang RP (1997) Appl Phys Lett 70:3308–3310
39. Hong ZS, Cao Y, Deng JF (2002) Mater Lett 52:34–38
40. Yao WT, Yu SH, Zhou Y, Jiang J, Wu QS, Zhang L, Jiang J (2005) J Phys Chem B 109:14011–14016
41. Wang H, Pan Q, Zhao J, Yin G, Zuo P (2007) J Power Sources 167:206–211
42. Gu Y, Jian F, Wang X (2008) Thin Solid Films 517:652–655
43. Wu GT, Wang CS, Zhang XB, Yang HS, Qi ZF, Li WZ (1998) J Power Sources 75:175–179
44. Grugeon S, Laruelle S, Herrera UR, Dupont LP, Tarascon JM (2001) J Electrochem Soc 148:A285–A292
45. Larcher D, Masquelier C, Bonnin D, Chabre Y, Masson V, Leriche JB, Tarascona JM (2003) J Electrochem Soc 150:A133–A139
46. Gao XP, Bao JL, Pan GL, Zhu HY, Huang PX, Wu F, Song DY (2004) J Phys Chem B 108:5547–5551
47. Poizot P, Laruelle S, Grugeon S, Dupont L, Tarascan JM (2000) Nature 407:496–499
48. Zou G, Li H, Zhang D, Xiong K, Dong C, Qian Y (2006) J Phys Chem B 110:1632–1637